Charge-transfer properties and electron dynamics in ferromagnetic CoS_2

Mahmoud Abdel-Hafiez,[1,2,3] Fredrik O. L. Johansson,[4,5,*] Anwesha Chakraborty,[6] Martin Pavelka,[7] Anirudha Ghosh,[8] D. A. Chareev,[9,10] A. N. Vasiliev,[11,12] Alexander Edström,[13,14,15] Anna Delin,[13,14,15] Olle Eriksson,[7,16] Debjani Karmakar,[6,7,17] and Dibya Phuyal[15,†]

[1]*Department of Applied Physics and Astronomy, University of Sharjah, P. O. Box 27272 Sharjah, United Arab Emirates*
[2]*Center for Advanced Materials Research, Research Institute of Sciences and Engineering, University of Sharjah, Sharjah 27272, United Arab Emirates*
[3]*Department of Physics, Faculty of Science, Fayoum University, Fayoum 63514, Egypt*
[4]*Institute Methods and Instrumentation for Synchrotron Radiation Research PS-ISRR, Helmholtz-Zentrum Berlin für Materialien und Energie, Albert-Einstein-Straße 15, 12489 Berlin, Germany*
[5]*Institut für Physik und Astronomie, Universität Potsdam, Karl-Liebknecht-Strasse 24-25, 14476 Potsdam, Germany*
[6]*Homi Bhabha National Institute, Anushaktinagar, Mumbai 400094, India*
[7]*Department of Physics and Astronomy, Uppsala University, Box 516, SE-75121 Uppsala, Sweden*
[8]*MAX IV Laboratory, Lund University, SE-221 00 Lund, Sweden*
[9]*Korzhinskii Institute of Experimental Mineralogy RAS, Chernogolovka 142432, Russia*
[10]*Ural Federal University, Ekaterinburg 620002, Russia*
[11]*National University of Science and Technology "MISiS," Moscow 119049, Russia*
[12]*Faculty of Physics, M.V. Lomonosov Moscow State University, Moscow 119991, Russia*
[13]*Swedish e-Science Research Center (SeRC), KTH Royal Institute of Technology, SE-10044 Stockholm, Sweden*
[14]*Wallenberg Initiative Materials Science for Sustainability (WISE), KTH Royal Institute of Technology, SE-10044 Stockholm, Sweden*
[15]*Department of Applied Physics, KTH Royal Institute of Technology, SE-11419 Stockholm, Sweden*
[16]*Wallenberg Initiative Materials Science for Sustainability (WISE), Uppsala University, SE-751 20 Uppsala, Sweden*
[17]*Technical Physics Division, Bhabha Atomic Research Centre, Trombay, Mumbai 400085, India*

(Received 24 February 2025; revised 3 September 2025; accepted 8 September 2025; published 14 October 2025)

We investigated the element-specific electronic structure and charge-carrier dynamics of a single-crystal ferromagnet CoS_2 with complementary x-ray spectroscopy techniques. Hard x-ray photoemission (HAXPES) is used to provide crucial information on the bulk electronic structure and chemical bonding in CoS_2 that is compared against the isoelectronic paramagnet $CoSe_2$. The Co 1*s* core-level line shows several satellite features for CoS_2, showing explicit charge-transfer processes and local screening of the core hole by S ligands, whereas no such features are observed in $CoSe_2$. The satellite structures indicate the electronic configuration of divalent Co^{2+} as a combination of $d^8\underline{L}$ and $d^9\underline{L}^2$ in addition to the nominal ionic d^7 state, where $\underline{L}$ represents an S 3*p* hole. We employ resonant Auger spectroscopy across the S *K*-edge for CoS_2 to obtain electron delocalization times to adjacent Co atomic sites. The fast carrier dynamics are attributed to strongly screened Coulomb interactions and hence a facile carrier delocalization. The strong hybridization formed between the Co 3*d* and S 3*p* states with pronounced charge-transfer character reflects a self-doped system with a finite density *n* of holes at the sulfur site ($\underline{L}^n$), in line with recent models that indicate a negative charge-transfer energy for CoS_2. In addition to HAXPES data, we also report on experimental and theoretical *L*-edge x-ray absorption and x-ray magnetic circular dichroism data for CoS_2 that demonstrate multiconfiguration effects in the excitation process. To enable a direct comparison of the experimental spectra, we used density functional theory calculations to obtain the projected density of states to describe the ground-state electronic structure. The existence of fast carrier dynamics and strong charge-transfer properties, demonstrated in this study, highlights the unique nature of CoS_2 with a wide potential in topological spintronics applications and integration in energy-related device platforms.

DOI: 10.1103/vg4c-h785

I. INTRODUCTION

Pyrite-type 3*d* transition-metal dichalcogenides MS_2 (M = Fe, Co, Ni, Cu) exhibit a wide variety of interesting electrical and magnetic properties [1–5]. Within this family,

*Present address: Department of Physics, Uppsala University, Box 516, SE-75121 Uppsala, Sweden.
†Contact author: dibya@kth.se

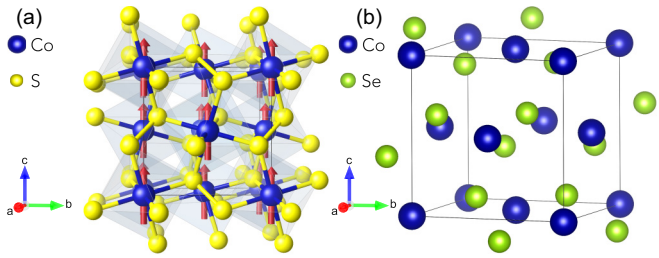

FIG. 1. Crystal structure of CoS_2 (a) and $CoSe_2$ (b). CoS_2 exhibits a pyrite crystal structure with a CoS_6 octahedra corner connected through S atoms which are also bonded to S atoms on neighboring octahedra, forming a S-S dimer bond. The magnetic moments for CoS_2 shown in red arrows are oriented along the (001) axis.

CoS_2 has been experimentally confirmed to be ferromagnetic and extensively studied for its magnetic properties and purported spin polarization [6–8]. Previous studies have suggested that CoS_2 is a half-metallic compound that is completely spin-polarized due to its low-spin state of Co^{2+} (configuration: $t_{2g}^6 e_g^1$) [9]. However, a previous comprehensive experimental and computational study revealed that CoS_2 hosts a minority-spin electron pocket that leads to a peak in the minority-spin density of states (DOS), which would make CoS_2 a minority-spin conductor [10]. This same study also detected a topological line node and Weyl points in the vicinity of the Fermi level (E_F), which gives rise to topological Fermi arc surface states that cross E_F. These novel attributes make CoS_2 a promising platform to probe topological phenomena in an accessible material that can be used in all sorts of electronic applications, from new magnetic memories to spin injector junctions [11]. In addition to its electrical and magnetic properties, CoS_2 has attracted significant interest as a promising anode material for both Li- and Na-ion batteries due to their high specific capacity [12]. More recently, both CoS_2 and $CoSe_2$ have been shown to be promising material systems in energy-related applications such as dye-sensitized solar cells (DSSCs), supercapacitors, and as electrocatalysts in an oxygen evolution reaction (OER) [13–15].

CoS_2 and $CoSe_2$ are pyrite-type cubic compounds that are regarded as isostructural within the same cubic space group ($Pa\bar{3}$), as shown in Fig. 1. In CoS_2, the Co atom is octahedrally coordinated by S ions, which also form S-S dimers [see Fig. 1(a)]. The Co $3d$ electrons are in the low spin state Co^{2+} with an ordered moment of $\sim 0.78 \mu_B$/Co, close to the value expected for an $S = 1/2$ system [8]. The general electronic structure of this system has previously been studied in detail using several varying density functional theory (DFT) methods, which yield contradictory ground-state properties, specifically with respect to its claimed half-metallic electronic structure [16,17].

Photoemission experiments have mainly focused on angle-resolved photoemission spectroscopy (ARPES) [18–21] or with photon energies limited to 100–1500 eV, where the inelastic mean free path of the photoelectron can be expected to be close to a minimum of 1 nm, resulting in a very surface-sensitive probe. In this context, it is highly important to elucidate the bulk electronic state and charge-transfer properties of CoS_2 by means of bulk-sensitive hard x-ray photoemission spectroscopy (HAXPES). A detailed understanding of the complex interaction between the formation of atomic multiplets and the effects of charge-transfer screening can be revealed through HAXPES [22,23], providing valuable information on the chemical bonding and electronic structure of CoS_2. A second aim in using HAXPES is to describe the charge-carrier dynamics of CoS_2 through an indirect method that relies on some other dynamic process to act as an internal clock using core-level photoemission processes. Using the core-hole-clock (CHC) method within the resonant Auger spectroscopy (RAS) framework with core excitations of the respective ions, the dynamics of electron delocalization to the neighboring atomic sites can be estimated [24–29]. This technique combines the chemical specificity of x-ray absorption with time resolution reaching into the subfemtosecond timescale.

Herein, we perform an extensive x-ray spectroscopy investigation to provide insight into the electronic structure properties, and we report specifically on the nature of charge-transfer effects and the role of ligand hybridization for cobalt disulfide (CoS_2) and its similar paramagnetic metal, cobalt diselenide ($CoSe_2$). Hard x-ray photoemission spectra reveal the presence of at least two satellite structures that can be identified as a ligand-to-metal charge transfer (LMCT). Here the relative magnitude of the LMCT is defined as $\Delta_{CT} = E(d^{n+1}\underline{L}^1) - E(d^n)$, where $\underline{L}$ is an S $3p$ hole. Resonant photoemission (ResPES) taken across the sulfur K-edge shows a partial density of states that lies far below the Fermi level (E_F), indicating that states close to E_F are largely composed of Co $3d$ character. RAS at the S K-edge was used to study the electron dynamics in CoS_2 from the CHC method, and it shows that the delocalization timescale of electrons in the conduction band can be estimated to be 150 as. Our experimental findings imply a negative charge transfer for CoS_2 established in previous reports, and they highlight the importance of ligand holes on its electronic structure and carrier dynamics.

II. EXPERIMENTAL AND COMPUTATIONAL DETAILS

High-quality single-crystal samples of CoS_2 and $CoSe_2$ measuring 5 mm × 5 mm × 0.5 mm were synthesized through the high-temperature flux method as previously reported [30]. Magnetic measurements were performed using a commercial SQUID magnetometer (MPMS XL, Quantum Design, USA) in a zero-field-cooled protocol with the magnetic field applied parallel to the plane of the sample. Field-dependent magnetization M versus H up to 7 T was performed in the paramagnetic (PM) phase (at 300 K) and the ferromagnetic (FM) phase (at 5 K).

X-ray magnetic circular dichroism (XMCD) and x-ray magnetic linear dichroism (XMLD) experiments were performed at the BOREAS beamline [31] at the ALBA synchrotron in Barcelona, Spain. The spectra were acquired by measuring the total electron yield (TEY) with an incidence angle that is parallel to the sample normal, where the surface normal is oriented along the (001) crystallographic direction. Data were collected at 2 K with an applied field of 2 T parallel to the sample normal. The low-temperature dichroic spectra

are obtained by calculating the difference between absorption spectra recorded with circularly (linear) right- (horizontal) and left-hand (vertical) polarized light, respectively. The obtained spectra were then normalized to an edge jump of 1 for each respective measurement.

Hard x-ray photoemission (HAXPES) measurements were made at the KMC-1 beamline [32] using the high kinetic energy end station HIKE [33] at Helmholtz-Zentrum Berlin (BESSY II). Electron kinetic energy was recorded with a Scienta R4000 hemispherical electron analyzer. X-ray absorption (XAS) was recorded in total fluorescence yield (TFY) using a Bruker fluorescence detector. The photon beam was linearly polarized horizontally and oriented perpendicular to the sample normal [(001) plane] for sensitivity to the in-plane electronic structure. By rotating the sample toward grazing incidence from the sample basal plane, the polarization can be chosen to vary the in-plane and out-of-plane components of the electronic structure. Measurements were performed at a base pressure 10^{-9} mbar range and 100 K for both samples. The binding energy was calibrated using the Fermi edge of an Au reference. To extract information from the Auger spectra, we first determined the line-shape parameters for the two separate features and determined them separately in photon energy regions where only one of them is present. The accuracy of the reported charge-transfer times is dependent on fitting uncertainties and choice of fitting parameters, and therefore we estimate this uncertainty to be $\Delta\chi^2 \leqslant \pm 15\%$.

The electronic structure was calculated using density functional theory (DFT) with two complementary approaches: (i) with the projector augmented wave (PAW) method [34,35] as implemented in VASP [36,37], and (ii) with an all-electron, full-potential method based on linear muffin-tin orbitals [38]. Spin-polarized calculations were performed in the local spin density approximation (LSDA) with the lattice parameter fixed to 5.52 Å, and Brillouin zone integration with a $7 \times 7 \times 7$ k-grid and Gaussian smearing of 0.05 eV. This leads to a net magnetic moment of $0.90\,\mu_B$ per Co atom, in excellent agreement with the experimentally reported value below.

The LSDA + U calculation incorporated a lattice parameter 5.52 Å and Hubbard U and J parameters having a value of 7 and 0.9 eV, respectively, and the exchange correlation functionals are Hedin-Lundqvist with von Barth–Hedin interpolation and random phase approximation (RPA) scaling. The Brillouin zone integrations were performed in a k-mesh of $12 \times 12 \times 12$ and Fermi smearing of 0.0068 eV. The Heisenberg intersite exchange parameter (J) is calculated by using Lichtenstein-Katsnelsen-Antropov-Gubanov (LKAG) formulation [39,40]. For the first few nearest neighbors (NNs), the values of the J-parameters are positive, bearing the values of 0.49 and 0.21 mRy for the first (3.76 Å) and second (5.32 Å) NN, indicating the prevalence of a long-range FM order within the system. The extracted critical temperature (T_c) for the FM-paramagnetic transition by using Monte Carlo simulation is ≈140 K, which is close to the experimentally measured T_c reported below.

To compare the obtained XAS and XMCD spectra, we have used the combined DFT and multiplet ligand field theory (DFT+MLFT) method to theoretically compute the x-ray spectra. In this method, the projection to the Co $3d$ orbitals is used to compute the projected density of states, the hybridization function, and the spin-orbit coupling parameters. To compute the $L_{2,3}$ edges, the core hole is created at the Co $2p$ core levels, and they are included in the solution of the single-impurity Anderson model (SIAM) [41,42]. The bare higher-order Slater-Condon integrals (F, G) corresponding to the L-edge x-ray spectroscopy are obtained with the corresponding modified basis sets, where the core hole is placed at the respective levels. After solving the SIAM, these integrals and hybridization functions are used to obtain the x-ray spectra. The double-counting corrections used in this calculation are formulated using the concept of charge-transfer energy [43]. Here, the inversion of the local Green's function, connecting the hopping parameters from impurity to bath, is used to calculate the hybridization of the projected Co $3d$ orbitals with the ligands. A combination of the DFT-derived single-particle Hamiltonian, the Coulomb interaction terms between the impurity $3d$ orbital and relevant bath states, and a $2p$ core spin-orbital state are used to construct the SIAM. The strong spin-orbit coupling of the core states leads to a splitting of the $L_{2,3}$ edges of the absorption spectrum. To take into account the effect of screening, the extracted bare F and G parameters are screened to 80% of their bare values. The zeroth-order parameters F_0^{dd} and F_0^{pd} are taken to be equal to the Hubbard U (6 eV) and $1.3U$ (7.8 eV) respectively. The values of the higher-order F and G parameters are $F_2^{dd} = 9.09$ eV, $F_4^{dd} = 5.84$ eV, $G_1^{pd} = 3.71$ eV, $G_3^{pd} = 2.11$ eV, and $F_2^{pd} = 5.11$ eV. The spin-orbit splittings of the core $2p$ and valence $3d$ levels are calculated as 9.85 and 0.09 eV respectively.

III. RESULTS

A. CoS_2 magnetization and XMCD

First, we establish the magnetic properties of single-crystal CoS_2 by combining conventional magnetization measurements with XMCD measurements. The ferromagnetic ordering temperature for CoS_2 is at 122 K with a sharp first-order-like phase transition as widely reported [8,44] and shown in Fig. 2(a). The magnetization hysteresis shows a saturation field of approximately 100 mT with a saturation magnetization of $\approx 0.9\mu_B$ shown in Fig. 2(b). The Co L-edge XAS with circular right (σ^+, CR) and left (σ^-, CL) -polarized light and the corresponding XMCD ($\sigma^+ - \sigma^-$) spectra were taken at 2 K and with an applied field of 2 T, well below the magnetic ordering temperature and above the saturation field as shown in Fig. 2(c). The spectral profile of the averaged XAS spectra is in good agreement with our calculated spectrum for a Co^{2+} state and consistent with a low-spin state configuration of $t_{2g}^6 e_g^1$ [top panel in Fig. 2(c)]. The features at 6–8 eV above the L_3 and L_2 edges are due to the transitions to the unoccupied Co $4s$ conduction bands, according to the calculated density of states in the corresponding energy region above the Fermi level that are well separated from the antibonding S $3s$ and Co e_g bands by an energy gap [1,45]. $CoSe_2$ shows a similar spectral profile to that of CoS_2 but with no magnetic dichroic signal. Using the sum-rule relations for spin $\langle m_S \rangle$ and orbital moment $\langle m_L \rangle$, we derived a spin moment of $\langle m_S \rangle \approx 0.78\,\mu_B$ and $\langle m_L \rangle \approx 0.047\,\mu_B$ for a total magnetic moment of $\langle m_{tot} \rangle = 0.83 \pm 0.083\,\mu_B$, in line with previously

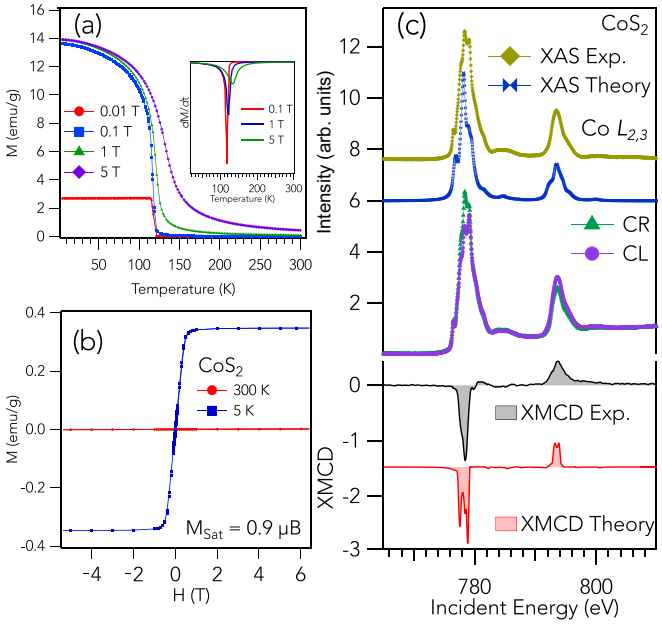

FIG. 2. (a) Temperature-dependent magnetization for CoS_2 with various applied fields. The inset shows a first derivative curve showing a ferromagnetic onset at $T_C \approx 122$ K. (b) M vs H curves at room temperature and 5 K measured perpendicular to the sample (001) plane. (c) Upper panel: The gold and blue curves are the averaged XAS experimental and calculated spectra, respectively. Middle panel: XMCD spectra of CoS_2 taken with right and left circularly polarized light at 2 K with an applied field of 2 T. Bottom panel: Experimental and calculated XMCD spectra. The calculated spectra are shifted vertically for clarity (for details, see the text).

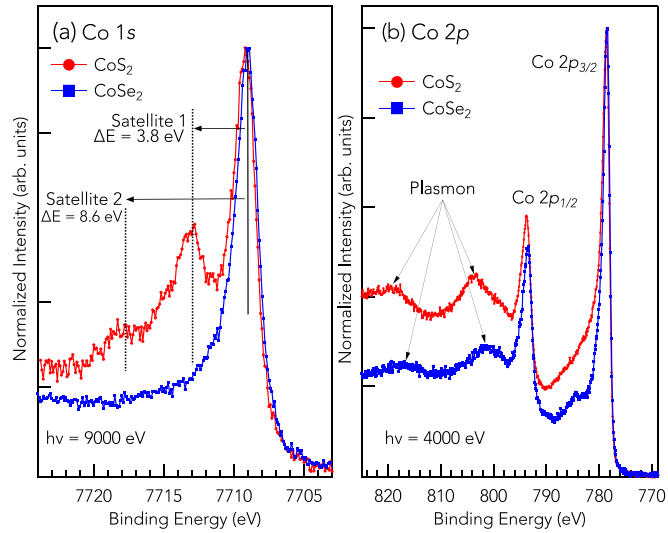

FIG. 3. (a) Co 1s HAXPES spectra taken at 9000 eV and at 100 K for both CoS_2 and $CoSe_2$. The dashed line indicates the energy separation of the satellite features for CoS_2 from the main line at 7709 eV. (b) Co 2p spectra taken at 4000 eV. Both sets of spectra are normalized to maximum intensity of the main line.

reported values [1,45] and in agreement with the experimental saturation moment of $0.9\mu_B$ shown in Fig. 2(b). These values are also in line with our calculated spin-magnetic moments of Co and S, which are 0.84 and $0.02\mu_B$, respectively, and a Co orbital contribution of $0.09\mu_B$. The magnitude of the local spin moment at the Co site is reduced to $0.78\mu_B$ compared to the ionic value $S = 1$ by strong Co $3d-$S $3p$ hybridization.

The calculated XAS spectra using the LSDA + U+MLFT method highlighted in Fig. 2(c) exhibits a branching ratio of the L_3 and L_2 edges equal to 3.5. This value deviates from the nominal value of 2, which is expected from an essentially uncorrelated, single determinant theory (such as LSDA). Hence, Fig. 2(c) points to a more complex electronic structure, where the excitation process that creates a hole in the Co 2p shell induces multiconfiguration effects, with multiplet features that are considered for both experimental and theoretical results.

B. Core-level HAXPES

Figure 3(a) shows the Co 1s core levels for both CoS_2 and $CoSe_2$ taken at 9000 eV and 100 K, which establishes some key ingredients in the electronic structure of the ground state. The CoS_2 1s spectrum yields an asymmetric main-line peak at 7709.2 eV binding energy (E_B) marked by a solid line and two satellite features at 3.8 and 8.6 eV separated from the main peak, respectively, as indicated by dashed lines. A sudden creation of a localized core hole triggers a dynamical charge response in the photoemission final states, which amounts to a charge transfer from surrounding ligands as well as distant Co ions to the excited Co site, conventionally referred to as charge-transfer (CT) screening [46]. The 1s excitation, with negligibly weak core-valence interaction, is thus better suited to examine and quantify the charge-transfer effect. The 1s main line can be ascribed to final states with a linear weighted combination of cd^7, $cd^8\underline{L}^1$, and $cd^9\underline{L}^2$, where c and $\underline{L}$ denote a 1s core hole and a hole in the valence band, respectively. The charge-transfer satellites correspond to a local screening of the core hole from S 3p bands.

While the 1s level should give rise to only one peak, the observation of multiple satellite peaks suggests that at least three different states contribute to the ground and final states in the photoemission process, namely the nominal valence of $3d^7$ (Co^{2+}) with at least two additional states [47]. The charge-transfer satellite peaks indicate a CoS_2 ground-state electronic structure with admixture with at least three different configurations to the ground state $3d^7$, $3d^8\underline{L}^1$, and $3d^9\underline{L}^2$ configurations, where the latter two represent ligand-hole contributions.

Both samples show an asymmetry in the 1s main line towards the high binding energy side that are fingerprints of local metallic screening from sulfur/selenium ligands in the final state [48,49]. The Co 1s spectrum for $CoSe_2$ exhibits no satellite features, which indicates that the charge-transfer screening process during the photoemission process is largely due to metallic screening from states at E_F rather than through adjacent ligands. The linear combination of multiple ground states for CoS_2 shows experimental evidence that links strong hybridization between Co 3d and S 3p states in contrast with $CoSe_2$, despite being nearly isostructural and isoelectronic. The Co 2p signal shown in Fig. 3(b) shows no distinguishable charge-transfer satellite peaks, which are obscured by the overlap of spin-orbit splits and multiplet effects common to 2p photoemission spectra [48]. The broad peaks found at

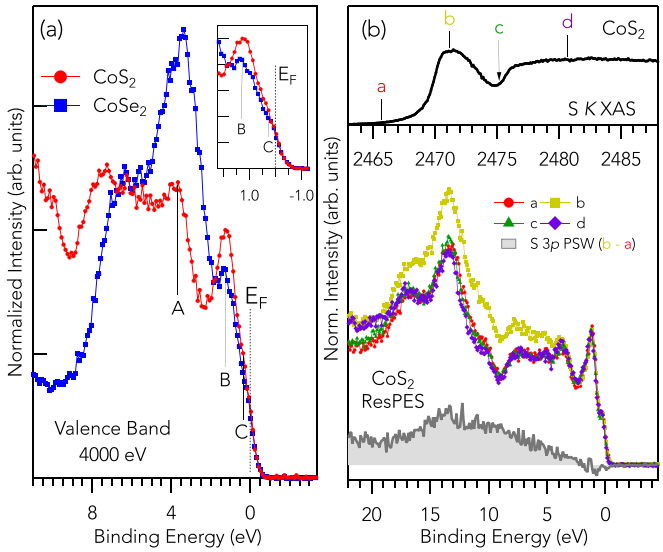

FIG. 4. (a) Valence-band spectra for CoS_2 and $CoSe_2$ taken with 4000 eV and 100 K and normalized to area. (b) Resonant photoemission spectroscopy (ResPES) taken at the S-K edge showing the S-K XAS (top panel) and the corresponding valence-band photoemission at selected excitation energies in the XAS spectrum.

805 eV E_B and 820 eV E_B for both samples are due to plasmon excitations, which were shown to obscure the $2p_{1/2}$ satellites in a previous Co $2p$ study [20].

C. Valence band

In Fig. 4(a) we compare the valence band for both CoS_2 and $CoSe_2$ measured at a photon energy of 4000 eV, corresponding to a photoemission probing depth of about 9 nm [50]. As noted above, the spectra measured at this photon energy are less surface-sensitive than previously reported valence-band ARPES data or spectra at lower photon energies ($h\nu < 1500$ eV). The spectra share similar gross features, namely peaks A and B positioned at similar E_B. On the lower-energy side, a tail extends from around a peak at 1.8 eV (labeled B) up to the Fermi level (E_F) with a small feature at 0.2 eV E_B (labeled C). The VB peaks labeled B and C towards the E_F are assigned to narrow Co t_{2g} and e_g bands as determined from previous photoemission findings [21,51]. For $CoSe_2$, for peaks labeled B and C at 1.8 and 0.2 eV, respectively, are assigned to Co $3d$ states with t_{2g} symmetry, while the shoulder peak C near E_F is attributed to Co $3d$ states with e_g symmetry [52]. Furthermore, the valence-band spectra for CoS_2 remain qualitatively the same when the photoemission signal is acquired at varying experimental geometries, suggesting similar orbital symmetry of the valence electrons and with a negligible dependence on in-plane and out-of-plane states (see Fig. S1 of the Supplemental Material [53]). This isotropic orbital occupation symmetry of the Co $3d$ shell is validated in the x-ray magnetic linear dichroism data (XMLD) (see Fig. S1 [53]) and exhibits a negligible linear dichroism signal for both CoS_2 and $CoSe_2$. To experimentally verify the role of sulfur states in the valence band, we performed resonant photoemission (ResPES) across the S K-edge. The top panel of Fig. 4(b) shows the XAS spectrum taken across the S K-edge along with colored labels that mark the excitation energies for the ResPES measurements. The bottom panel in Fig. 4(b) shows the valence-band spectra in the S $1s-3p$ core absorption region ($h\nu = 2460-2490$ eV). These spectra were normalized by the photoelectron intensities of the shallow Co $3s$ core level, which does not contribute to the resonant process. No marked change near the valence-band edge (3–0 eV E_B) is found and is energy-independent across the different energies. Notably, the enhanced spectra taken at the S K resonance (2475 eV) are located in the range of 20–3 eV, and they are classified with S $3p$ and S $3s$ character, with peaks at 17 and 13 eV corresponding to S $3s$ bonding and antibonding states from S-S dimer pairs in CoS_2, similar to the states found in recent HAXPES spectra for NiS_2 [3] and CuS_2 [5]. The difference between on-resonance (2475 eV) and off-resonance (2470 eV), as depicted by the gray shaded area in the bottom panel, reflects the partial spectral weight (PSW) of S $3p$ states. This result signifies the presence of dominant Co $3d$ partial DOS near the VB edge with little S contribution. It is worth noting that previous studies have identified CoS_2 to be a negative charge-transfer compound [2,54] driven largely by a p-band that is metallic and self-doped with holes. Although S $3p$ spectral intensities are not pronounced at the valence-band edge from this spectra, recent reports suggest that ligand hole states are accommodated in the S antibonding orbitals that lie just below and above the Fermi level [2,3,5]. The strong hybridization between Co $3d-$S $3p$ states near the Fermi level will be presented later.

D. Resonant Auger spectroscopy

We access the site- and element-specific ultrafast carrier dynamics in CoS_2 by monitoring competing decay channels following an x-ray absorption from the S $1s$ level into the conduction band. This method uses an intrinsic timescale due to the core-hole lifetime (Γ_{ch}) of a specific atomic level, which allows us to interpret electron-electron correlation effects and their role in excited electron dynamics. Figure 5(a) illustrates the principles of resonant Auger processes with several possible relaxation pathways after resonant excitation. If the incident x-ray photon energy $\hbar\omega$ exceeds the S $1s$ ionization threshold (nonresonant case), a $1s$ photoelectron is ejected into the continuum, followed by electron relaxation in the form of normal Auger decay, where one $2p$ electron fills the S $1s$ vacancy, while another $2p$ electron is ejected as a normal Auger electron (NA) that is independent of the incident photon energy, resulting in a two-hole final state.

In contrast, the resonant case can proceed with the promoted electron remaining in the excited state during the subsequent relaxation process, leaving a final state with two holes and one spectator Auger (SA) electron. Here, a linear relation can be observed between the energy of the incident photon and the spectator Auger electron kinetic energy. If the excited electron delocalizes during the relaxation process on a timescale shorter than the core-hole lifetime (a few femtoseconds), a two-hole zero-electron final state is reached with the Auger electron feature identical to the normal Auger decay case, designated as the charge-transfer channel. The competitive kinetics of electron delocalization and known core-hole decay manifest themselves directly in the relative intensities

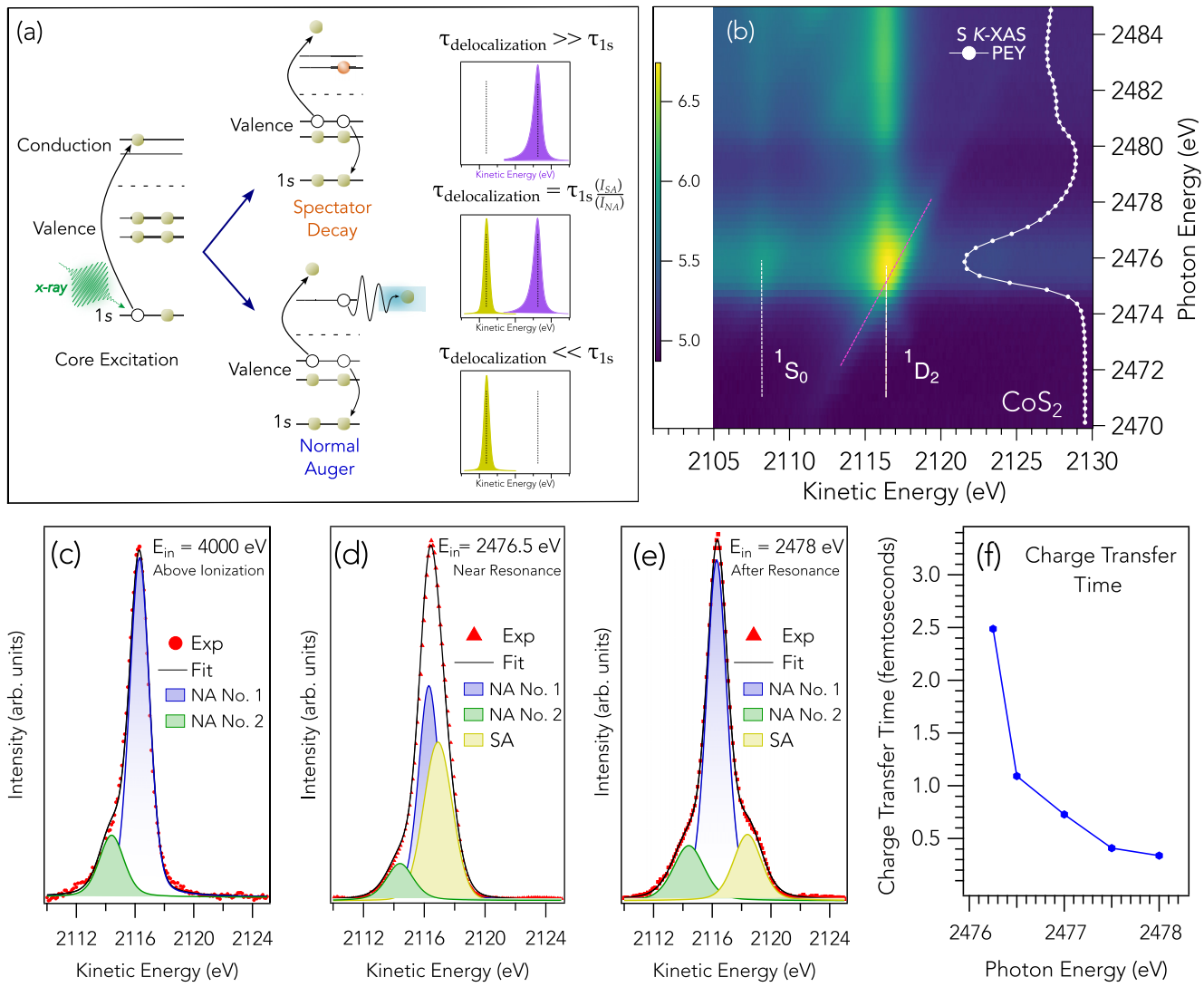

FIG. 5. (a) Schematic overview of the working principle of the core-hole clock spectroscopy where photoexcitation drives several different Auger processes along with charge delocalization or charge-transfer processes. Depending on the core-hole lifetime, τ_{1s}, and the delocalization time, $\tau_{\text{delocalization}}$, different spectator and normal Auger electron signal-intensity ratios are obtained. (b) Resonant Auger intensity maps of S *KLL* photoemission for CoS_2. (c)–(e) Resonant photoemission spectra of S *KLL* are recorded at the photon energy at 4000, 2476, and 2478 eV, respectively. The experimental spectra are shown in red dotted markers, the overall fit are in black solid lines, fits for normal Auger (NA) are in green and purple, and the resonant spectator Auger (SA) that linearly disperses is in gold. (f) Calculated charge-transfer times plotted as a function of incident energy.

of the resonantly shifted spectator Auger (SA) and normal Auger (NA) features. This approach is used to investigate the ultrafast electron dynamics in CoS_2.

Figure 5(b) shows the resonant contour plot of Auger emission intensity as a function of photon excitation energy across the S *K*-edge. The Auger map shows two prominent structures, namely the KL_2L_2 ($^1S_0$) and the KL_2L_3 ($^1D_2$) Auger channels at 2107 and 2116 eV kinetic energy, respectively [27,28,55,56]. These features appear at constant kinetic energy and are indicated by vertical dashed lines in Fig. 5(b), whereas direct incoherent features disperse with excitation energy as indicated by a dashed purple line. The intensity map in Fig. 5(b) shows a strong resonant enhancement of the sulfur $^1D_2$ Auger feature when the photon energy is tuned to the absorption maximum, shown on the right axis of Fig. 5(b). The distribution between the different channels and their relative intensities is directly related to the electronic lifetimes and charge transfer in the conduction band of CoS_2 to adjacent atomic sites. The delocalization time is obtained directly from the ratio of the integrated spectator Auger and normal Auger components to the S KL_2L_3 ($^1D_2$) feature as

$$\tau_{\text{deloc}} = \frac{I_{\text{SA}}}{I_{\text{NA}}} \times \tau_{\text{S 1s}}, \tag{1}$$

where τ_{1s} is the core-hole lifetime of *S* 1*s*, and I_{SA} and I_{NA} are the intensities of the spectator and normal Auger contributions respectively. The natural lifetime of the S 1*s* core hole is calculated to be $\tau_{1s} = 1.27$fs [57]. The normal Auger spectrum taken at a photon energy of 4000 eV was fitted far above the ionization threshold to obtain a fixed

energy position for the normal Auger peak (2116.3 eV), as shown in Fig. 5(c). Figure 5(d) shows the Auger spectra at 2476.5 eV, which corresponds to just after the absorption maximum in the S K-XAS curve on the right axis of Fig. 5(b). The intensity of the spectator Auger feature is nearly that of the normal Auger feature, indicating a long-lived excited electron that screens the core-hole decay. At 2478 eV, the spectator Auger is shifted by an equal amount in photon energy in comparison with the spectra taken near resonance at 2476.5 eV (spectator shift of 1.5 eV).

Our spectral decomposition analysis and fits are repeated from near resonance to after resonance to yield the evolution of delocalization time using Eq. (1) and plotted at selected energies in Fig. 5(f). After resonance at 2476.5 eV, the charge transfer is observed to exhibit normal exponential decay with a higher excitation energy. The intensities of I_{SA} and I_{NA} vary over the investigated photon range (2470–2485 eV) where a large intensity I_{SA} reflects long-lived excited states, and a smaller intensity of I_{SA} indicates fast electron delocalization. Near resonance (2476.5 eV), charge delocalization times have an upper bound of 3 fs. At regions past the absorption maximum, charge delocalization times are much faster by at least an order of magnitude, i.e., $\tau_{deloc} = 100-300$ as. This timescale measured by the CHC method reflects the decoupling time of an excited electron from a specific atomic site, which is useful for analyzing the transport properties in real devices.

IV. DISCUSSION

To understand the origin of the energy-dependent dynamics and the charge-transfer properties of CoS_2, we turn to electronic structure calculations. We have calculated the density of states for CoS_2 and $CoSe_2$ using the LSDA methodology as shown in Fig. 6. These results agree with previous band structure calculations [1,7,10,58] and lead to a peak in the minority-spin DOS, rendering CoS_2 a minority-spin conductor. The broadband of 6 eV width between -8 and -2 eV consists mainly of S $3p$ states [see Fig. 6(b)], which is a mixture of $3p\sigma$ and $3p\pi$ states [1]. Figure 6(c) shows Co t_{2g} bands that are located between 1 and 3 eV below the Fermi energy E_F while Co e_g bands cross E_F with a relatively large bandwidth of about 2.5 eV due to strong hybridization with the S $3p$ band. This strong hybridization and metallic states at the Fermi level from neighboring S $3p$ bands effectively screen the Co $1s$ core hole and produce the charge-transfer features seen in Fig. 3(a). In contrast, $CoSe_2$ only exhibits an asymmetry in the Co $1s$ main line that is due to screening from metallic states at the Fermi level that screen the core hole rather than a direct ligand-to-metal charge transfer. $CoSe_2$ has a much larger electron correlation (U), thereby suppressing the charge fluctuations between the Co $3d$ and ligand sulfur $3p$ orbitals despite its comparable orbital hopping integral [51]. Furthermore, it has been shown that CoS_2 has enhanced spin-dependent electron correlation effects on the electric structure in the vicinity of the half-metallic state. Since there are eight S atoms in the unit cell, this implies that two $3p$ orbitals per S are fully filled and one $3p$ orbital per S takes part in the formation of S-S dimers by making a covalent bond. Indeed, the four antibonding S $3p$ bands can be found above the

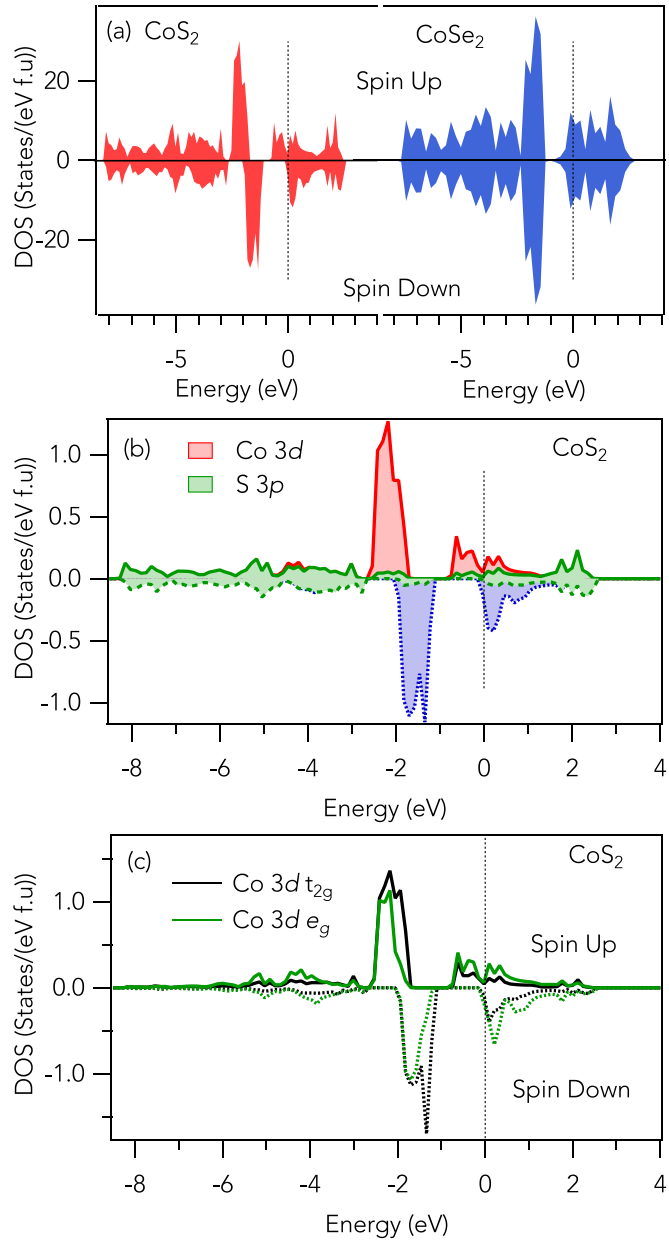

FIG. 6. (a) Electronic density of states calculated for CoS_2 and $CoSe_2$. (b) Partial density of states (DOS) for CoS_2 from Co and S sites. (c) Co $3d$ orbitally resolved DOS, and their corresponding t_{2g} and e_g states.

Fermi level or partially crossing it [58]. The formal oxidation state assignments would suggest valences of 4− for the S_2 and therefore 4+ for the cations. However, it is plausible that the Co ions in the Co^{2+} state are self-doped with sulfur $3p$ holes [2]. This was previously suggested to originate from the highly polarizable nature of the S_2^{2-} ligand, which effectively screens the strong core-hole potential [59].

Laila *et al.* [2] recently reported charge-transfer multiplet cluster model calculations on a family of pyrites including CoS_2 that considered all electronic configurations in the initial and final states to simulate their XAS spectra, specifically the appropriate combinations of $3d^n$ and $3d^{n+1}\underline{L}^n$ basis states and their relevant electronic parameters, such as crystal-field split-

ting (10_{Dq}), on-site $d-d$ Coulomb repulsion energy (U_{dd}), the metal $3d-$S $3p$ hybridization strength ($pd\sigma$), and lastly the charge-transfer energy between the $3d^n$ and $3d^{n+1}\underline{L}^n$ states (Δ_{CT}). Their results show a suitable match to the experimental spectra when using a negative charge-transfer energy of $\Delta_{CT} = -1.5$ eV for CoS_2. Similarly, related pyrites such as FeS_2 and NiS_2 were also shown to have negative charge-transfer character with explicit self-doped ligand holes [2,60]. This suggests that the overlap between the cobalt d^n and $d^{n+1}\underline{L}^n$ configurations becomes strong and the contribution of the $d^{n+1}\underline{L}^n$ configuration to the ground state is considerable [61]. Our experimental valence band and DFT calculations show that the edges of both valence and conduction bands are of hybridized S $3p$ Co $3d$ character. This indicates a $p-p$ type lowest energy excitation in the Zaanen-Sawatzky-Allen phase diagram [62]. In this scenario, transition-metal compounds with no gap in the p-p excitations are effectively self-doped by holes [2].

V. CONCLUSION

In summary, we have studied the bulk electronic structure of CoS_2 and related $CoSe_2$ by means of comprehensive soft and hard x-ray spectroscopy methods. Bulk sensitive HAXPES data results enabled us to observe distinct satellite features that point to intrinsic multiple ground states in the electronic structure. In CoS_2, the Co $1s$ spectrum exhibits spectral features that are a signature of metallic and ligand-metal CT screening upon core-level excitation. The experimental XAS/XMCD results for CoS_2 were found to be correctly reproduced in terms of relative intensities and energy position. These results agree with several recent experimental and theoretical reports on a negative charge-transfer energy for CoS_2, whereby self-doping of the ligand S band is responsible for the multiple CT satellites. Furthermore, the valence-band spectrum confirms a large spectral weight of Co $3d$ states towards the valence-band maximum with a small spectral weight of S states. The dynamical charge-transfer process was investigated through the core-hole clock technique via the resonant Auger process to obtain charge-carrier delocalization times, and it provides information on charge transport properties in real devices.

ACKNOWLEDGMENTS

This work is supported by the Swedish Research Council through Grant No. 2020-0068. D.P., M.P., and A.G. acknowledge the ALBA Synchrotron (Proposal: 2020094545) and BESSY (Proposal: 201-09341-ST/R-1.1-P) II for providing beamtime, and to their staff scientists for their support and discussion during beamtime. F.O.L.J acknowledges support from the Swedish Research Council (Grant No. 2020-06409) and the ÅForsk foundation (Grant No. 23-693). A.E. acknowledges financial support from the Swedish Research Council (VR -2022-04720), ÅForsk (22-441), the Göran Gustafsson Foundation, and Swedish e-Science Research Council (SeRC). M.A.H. acknowledges support by Deutsche Forschungsgemeinschaft (DFG) under Germany's Excellence Strategy EXC2181/1-390900948 (The Heidelberg STRUCTURES Excellence Cluster). Financial support from the Swedish Research Council (Vetenskapsrådet, VR) Grants No. 2016-05980, No. 2019-05304, and No. 2024-04986, and the Knut and Alice Wallenberg Foundation Grants No. 2018.0060, No. 2021.0246, and No. 2022.0108 is acknowledged. D.A.C. acknowledges RSCF Grant No. 25-12-00028 for crystal growth. The Wallenberg Initiative Materials Science for Sustainability (WISE) funded by the Knut and Alice Wallenberg Foundation is also acknowledged. O.E. also acknowledges support from STandUPP and eSSENCE. Crystal growth funded by the Ministry of Science and Higher Education of the Russian Federation and Ural Federal University Program of Development within the Priority-2030 and FMUF-2022-0002. The computations/data handling were enabled by resources provided by the National Academic Infrastructure for Supercomputing in Sweden (NAISS), partially funded by the Swedish Research Council through Grant Agreement No. 2022-06725. A.C. and D.K. acknowledge BARC supercomputing facility for computational resources.

DATA AVAILABILITY

The data that support the findings of this article are not publicly available. The data are available from the authors upon reasonable request.

[1] V. N. Antonov, O. V. Andryushchenko, A. P. Shpak, A. N. Yaresko, and O. Jepsen, Electronic structure, optical spectra, and x-ray magnetic circular dichroism in CoS_2, Phys. Rev. B **78**, 094409 (2008).

[2] A. Z. Laila, T. L. Nguyen, R. Furui, A. Shelke, F.-H. Chang, H.-J. Lin, C.-T. Chen, S. Hamamoto, A. Fujimori, T. Mizokawa, A. Chainani, and A. Yamamoto, Comparative study of a high-entropy metal disulfide and its parent compounds using x-ray absorption spectroscopy, Phys. Rev. B **109**, 195129 (2024).

[3] K. Fujinuma, D. Takegami, T. Higo, A. Melendez-Sans, G. Poelchen, M. Yoshimura, K.-D. Tsuei, S. Nakatsuji, L. H. Tjeng, and T. Mizokawa, Bulk Mott gap and S$3s$/$3p$ spectral distribution in pyrite-type NiS_2 revealed by hard x-ray photoemission spectroscopy, Phys. Rev. B **110**, 125136 (2024).

[4] D. Wang, X. Chen, and B. Sanyal, Unraveling complex magnetism in two-dimensional FeS_2, Phys. Rev. B **104**, 245410 (2021).

[5] K. Fujinuma, D. Takegami, A. Melendez-Sans, M. Yoshimura, K.-D. Tsuei, R. Higashinaka, T. D. Matsuda, Y. Aoki, M. Hedo, Y. Ōnuki, L. H. Tjeng, and T. Mizokawa, Effect of S $3p$ and Se $4p$ holes on charge fluctuations in pyrite-type CuS_2 and $CuSe_2$ revealed by hard x-ray photoemission spectroscopy, Phys. Rev. B **111**, 115147 (2025).

[6] S. K. Kwon, S. J. Youn, and B. I. Min, Itinerant ferromagnetism in half-metallic CoS_2, Phys. Rev. B **62**, 357 (2000).

[7] A. Teruya, F. Suzuki, D. Aoki, F. Honda, A. Nakamura, M. Nakashima, Y. Amako, H. Harima, M. Hedo, T. Nakama, and Y. Ōnuki, Large cyclotron mass and large ordered moment in

ferromagnet CoS_2 compared with paramagnet $CoSe_2$, J. Phys. Soc. Jpn. **85**, 064716 (2016).

[8] A. Teruya, F. Suzuki, D. Aoki, F. Honda, A. Nakamura, M. Nakashima, Y. Amako, H. Harima, K. Uchima, M. Hedo, T. Nakama, and Y. Ōnuki, Fermi surface and magnetic properties in ferromagnet CoS_2 and paramagnet $CoSe_2$ with the pyrite-type cubic structure, J. Phys.: Conf. Ser. **807**, 012001 (2017).

[9] P. J. Brown, K.-U. Neumann, A. Simon, F. Ueno, and K. R. A. Ziebeck, Magnetization distribution in CoS_2; Is it a half metallic ferromagnet? J. Phys.: Condens. Matter **17**, 1583 (2005).

[10] N. B. M. Schröter, I. Robredo, S. Klemenz, R. J. Kirby, J. A. Krieger, D. Pei, T. Yu, S. Stolz, T. Schmitt, P. Dudin, T. K. Kim, C. Cacho, A. Schnyder, A. Bergara, V. N. Strocov, F. de Juan, M. G. Vergniory, and L. M. Schoop, Weyl fermions, Fermi arcs, and minority-spin carriers in ferromagnetic CoS_2, Sci. Adv. **6**, eabd5000 (2020).

[11] I. Robredo, N. B. M. Schröter, A. Reyes-Serrato, A. Bergara, F. de Juan, L. M. Schoop, and M. G. Vergniory, Theoretical study of topological properties of ferromagnetic pyrite CoS_2, J. Phys. D **55**, 304004 (2022).

[12] Y. Xiao, S. H. Lee, and Y. Sun, The application of metal sulfides in sodium ion batteries, Adv. Energy Mater. **7**, 1601329 (2017).

[13] S. Y. S. Jaberi, A. Ghaffarinejad, Z. Khajehsaeidi, and A. Sadeghi, The synthesis, properties, and potential applications of CoS_2 as a transition metal dichalcogenide (TMD), Int. J. Hydrogen Energy **48**, 15831 (2023).

[14] X. Zheng, X. Han, Y. Cao, Y. Zhang, D. Nordlund, J. Wang, S. Chou, H. Liu, L. Li, C. Zhong, Y. Deng, and W. Hu, Identifying dense $NiSe_2/CoSe_2$ heterointerfaces coupled with surface high-valence bimetallic sites for synergistically enhanced oxygen electrocatalysis, Adv. Mater. **32**, 2000607 (2020).

[15] Y. Dou, C.-T. He, L. Zhang, H. Yin, M. Al-Mamun, J. Ma, and H. Zhao, Approaching the activity limit of $CoSe_2$ for oxygen evolution via Fe doping and Co vacancy, Nat. Commun. **11**, 1664 (2020).

[16] N. Wu, Y. B. Losovyj, D. Wisbey, K. Belashchenko, M. Manno, L. Wang, C. Leighton, and P. A. Dowben, The electronic band structure of CoS_2, J. Phys.: Condens. Matter **19**, 156224 (2007).

[17] T. Shishidou, A. J. Freeman, and R. Asahi, Effect of GGA on the half-metallicity of the itinerant ferromagnet CoS_2, Phys. Rev. B **64**, 180401(R) (2001).

[18] T. Takahashi, Y. Naitoh, T. Sato, T. Kamiyama, K. Yamada, H. Hiraka, Y. Endoh, M. Usuda, and N. Hamada, Para- to ferromagnetic phase transition of CoS_2 studied by high-resolution photoemission spectroscopy, Phys. Rev. B **63**, 094415 (2001).

[19] A. E. Bocquet, K. Mamiya, T. Mizokawa, A. Fujimori, T. Miyadai, H. Takahashi, M. Môri, and S. Suga, Electronic structure of $3d$ transition metal pyrites MS_2 (M = Fe, Co or Ni) by analysis of the M $2p$ core-level photoemission spectra, J. Phys.: Condens. Matter **8**, 2389 (1996).

[20] A. E. Bocquet, T. Mizokawa, T. Saitoh, H. Namatame, and A. Fujimori, Electronic structure of $3d$ -transition-metal compounds by analysis of the $2p$ core-level photoemission spectra, Phys. Rev. B **46**, 3771 (1992).

[21] A. Fujimori, K. Mamiya, T. Mizokawa, T. Miyadai, T. Sekiguchi, H. Takahashi, N. Môri, and S. Suga, Resonant photoemission study of pyrite-type NiS_2, CoS_2, and FeS_2, Phys. Rev. B **54**, 16329 (1996).

[22] A. Hariki, T. Uozumi, and J. Kuneš, LDA+DMFT Approach to core-level spectroscopy: Application to $3d$ transition metal compounds, Phys. Rev. B **96**, 045111 (2017).

[23] D. Phuyal, S. Mukherjee, S. K. Panda, G. J. Man, K. Simonov, L. Simonelli, S. M. Butorin, H. Rensmo, and O. Karis, Nonlocal interactions in the double perovskite Sr_2FeMoO_6 from core-level x-ray spectroscopy, J. Phys. Chem. C **125**, 11249 (2021).

[24] P. A. Brühwiler, O. Karis, and N. Mårtensson, Charge-transfer dynamics studied using resonant core spectroscopies, Rev. Mod. Phys. **74**, 703 (2002).

[25] A. Föhlisch, P. Feulner, F. Hennies, A. Fink, D. Menzel, D. Sanchez-Portal, P. M. Echenique, and W. Wurth, Direct observation of electron dynamics in the attosecond domain, Nature (London) **436**, 373 (2005).

[26] M. N. Piancastelli, G. Goldsztejn, T. Marchenko, R. Guillemin, R. K. Kushawaha, L. Journel, S. Carniato, J.-P. Rueff, D. Céolin, and M. Simon, Core-hole-clock spectroscopies in the tender x-ray domain, J. Phys. B **47**, 124031 (2014).

[27] F. O. L. Johansson, U. B. Cappel, M. Fondell, Y. Han, M. Gorgoi, K. Leifer, and A. Lindblad, Tailoring ultra-fast charge transfer in MoS_2, Phys. Chem. Chem. Phys. **22**, 10335 (2020).

[28] F. O. L. Johansson, X. Chen, O. Eriksson, B. Sanyal, and A. Lindblad, Interlayer charge transfer in tin disulphide: Orbital anisotropy and temporal aspects, Phys. Rev. B **102**, 035165 (2020).

[29] C. N. Eads, D. Bandak, M. R. Neupane, D. Nordlund, and O. L. A. Monti, Anisotropic attosecond charge carrier dynamics and layer decoupling in quasi-2D layered SnS_2, Nat. Commun. **8**, 1369 (2017).

[30] Y. Li, T. Polakovic, J. Curtis, S. L. Shumlas, S. Chatterjee, S. Intikhab, D. A. Chareev, O. S. Volkova, A. N. Vasiliev, G. Karapetrov, and J. Snyder, Tuning the activity/stability balance of anion doped CoS_xSe_{2-x} dichalcogenides, J. Catal. **366**, 50 (2018).

[31] A. Barla, J. Nicolás, D. Cocco, S. M. Valvidares, J. Herrero-Martín, P. Gargiani, J. Moldes, C. Ruget, E. Pellegrin, and S. Ferrer, Design and performance of BOREAS, the beamline for resonant x-ray absorption and scattering experiments at the ALBA synchrotron light source, J. Synch. Radiat. **23**, 1507 (2016).

[32] F. Schaefers, M. Mertin, and M. Gorgoi, KMC-1: A high resolution and high flux soft x-ray beamline at BESSY, Rev. Sci. Instrum. **78**, 123102 (2007).

[33] M. Gorgoi, S. Svensson, F. Schäfers, G. Öhrwall, M. Mertin, P. Bressler, O. Karis, H. Siegbahn, A. Sandell, H. Rensmo, W. Doherty, C. Jung, W. Braun, and W. Eberhardt, The high kinetic energy photoelectron spectroscopy facility at BESSY progress and first results, Nucl. Instrum. Methods Phys. Res. Sect. A **601**, 48 (2009).

[34] G. Kresse and D. Joubert, From ultrasoft pseudopotentials to the projector augmented-wave method, Phys. Rev. B **59**, 1758 (1999).

[35] G. Kresse and J. Furthmüller, Efficiency of ab-initio total energy calculations for metals and semiconductors using a plane-wave basis set, Comput. Mater. Sci. **6**, 15 (1996).

[36] G. Kresse and J. Hafner, *Ab initio* molecular-dynamics simulation of the liquid-metal–amorphous-semiconductor transition in germanium, Phys. Rev. B **49**, 14251 (1994).

[37] G. Kresse and J. Hafner, *Ab initio* molecular dynamics for liquid metals, Phys. Rev. B **47**, 558 (1993).

[38] J. M. Wills, O. Eriksson, P. Andersson, A. Delin, O. Grechnyev, and M. Alouani, *Full-Potential Electronic Structure Method* (Springer, Berlin, 2010), Vol. 167.

[39] A. Liechtenstein, M. Katsnelson, V. Antropov, and V. Gubanov, Local spin density functional approach to the theory of exchange interactions in ferromagnetic metals and alloys, J. Magn. Magn. Mater. **67**, 65 (1987).

[40] M. N. Hasan, R. Bharati, J. Hellsvik, A. Delin, S. K. Pal, A. Bergman, S. Sharma, I. D. Marco, M. Pereiro, P. Thunström, P. M. Oppeneer, O. Eriksson, and D. Karmakar, Magnetism in AV_3Sb5 (A = Cs, Rb, and K): Origin and consequences for the strongly correlated phases, Phys. Rev. Lett. **131**, 196702 (2023).

[41] F. Sorgenfrei, M. Alouani, J. Schött, H. J. Jönsson, O. Eriksson, and P. Thunström, Theory of x-ray absorption spectroscopy for ferrites, Phys. Rev. B **109**, 115126 (2024).

[42] M. N. Hasan, F. Sorgenfrei, N. Pan, D. Phuyal, M. Abdel-Hafiez, S. K. Pal, A. Delin, P. Thunström, D. D. Sarma, O. Eriksson, and D. Karmakar, Re-dichalcogenides: Resolving conflicts of their structure–property relationship, Adv. Phys. Res. **1**, 2200010 (2022).

[43] J. Lüder, J. Schött, B. Brena, M. W. Haverkort, P. Thunström, O. Eriksson, B. Sanyal, I. D. Marco, and Y. O. Kvashnin, Theory of l-edge spectroscopy of strongly correlated systems, Phys. Rev. B **96**, 245131 (2017).

[44] M. Otero-Leal, F. Rivadulla, M. García-Hernández, A. Piñeiro, V. Pardo, D. Baldomir, and J. Rivas, Effect of spin fluctuations on the thermodynamic and transport properties of the itinerant ferromagnet CoS_2, Phys. Rev. B **78**, 180415(R) (2008).

[45] E. Mijit, K. Chen, F. Choueikani, A. Di Cicco, and F. Baudelet, Collapse of itinerant ferromagnetism in CoS_2 under pressure: An x-ray absorption spectroscopy study, Phys. Rev. B **98**, 184423 (2018).

[46] F. M. D. Groot and A. Kotani, *Core Level Spectroscopy of Solids* (CRC, Boca Raton, FL, 2008).

[47] P. Miedema, F. Borgatti, F. Offi, G. Panaccione, and F. de Groot, Iron 1s x-ray photoemission of Fe_2O_3, J. Electron Spectrosc. Relat. Phenom. **203**, 8 (2015).

[48] M. Ghiasi, A. Hariki, M. Winder, J. Kuneš, A. Regoutz, T. L. Lee, Y. Hu, J. P. Rueff, and F. M. D. Groot, Charge-transfer effect in hard x-ray 1s and 2p photoemission spectra: LDA+DMFT And cluster-model analysis, Phys. Rev. B **100**, 075146 (2019).

[49] T. Yamaguchi, K. Higashi, A. Regoutz, Y. Takahashi, M. Lazemi, Q. Che, F. M. F. de Groot, and A. Hariki, Atomic multiplet and charge transfer screening effects in 1s and 2p core-level x-ray photoelectron spectra of early 3d transition-metal oxides, Phys. Rev. B **109**, 205143 (2024).

[50] S. Tanuma, C. J. Powell, and D. R. Penn, Calculations of electron inelastic mean free paths (IMFPS). IV. Evaluation of calculated IMFPs and of the predictive IMFP formula TPP-2 for electron energies between 50 and 2000 eV, Surf. Interface Anal. **20**, 77 (1993).

[51] H. Sato, F. Nagasaki, Y. Kani, S. Senba, Y. Ueda, A. Kimura, and M. Taniguchi, Electronic structure of $CoSe_2$ studied by photoemission spectroscopy using synchrotron radiation, Solid State Commun. **118**, 563 (2001).

[52] H. Fujiwara, K. Terashima, J. Otsuki, N. Takemori, H. O. Jeschke, T. Wakita, Y. Yano, W. Hosoda, N. Kataoka, A. Teruya, M. Kakihana, M. Hedo, T. Nakama, Y. Ōnuki, K. Yaji, A. Harasawa, K. Kuroda, S. Shin, K. Horiba, H. Kumigashira *et al.*, Anomalously large spin-dependent electron correlation in the nearly half-metallic ferromagnet CoS_2, Phys. Rev. B **106**, 085114 (2022).

[53] See Supplemental Material at http://link.aps.org/supplemental/10.1103/vg4c-h785 for additional figures related to the spherical symmetry of CoS_2 and $CoSe_2$ from XMLD and HAXPES experiments.

[54] E. Pavarini, E. Koch, J. van den Brink, and G. Sawatzky, *Quantum Materials: Experiments and Theory* (Verlag des Forschungszentrum, Jülich, 2016), pp. 18–24.

[55] F. O. L. Johansson, M. Ivanović, S. Svanström, U. B. Cappel, H. Peisert, T. Chassé, and A. Lindblad, Femtosecond and attosecond electron-transfer dynamics in PCPDTBT:PCBM Bulk heterojunctions, J. Phys. Chem. C **122**, 12605 (2018).

[56] R. Püttner, D. Céolin, R. Guillemin, R. K. Kushawaha, T. Marchenko, L. Journel, M. N. Piancastelli, and M. Simon, Detailed analysis of shake structures in the KLL auger spectrum of H_2S, Phys. Rev. A **93**, 042501 (2016).

[57] J. Campbell and T. Papp, Width of the atomic K-$N7$ levels, At. Data Nucl. Data Tables **77**, 1 (2001).

[58] A. Mukherjee and A. Subedi, Minority-spin conducting states in Fe substituted pyrite CoS_2, J. Phys.: Condens. Matter **36**, 025501 (2024).

[59] W. Folkerts, G. A. Sawatzky, C. Haas, R. A. de Groot, and F. U. Hillebrecht, Electronic structure of some 3d transition-metal pyrites, J. Phys. C **20**, 4135 (1987).

[60] R. J. Green and G. A. Sawatzky, Negative charge transfer energy in correlated compounds, J. Phys. Soc. Jpn. **93**, 121007 (2024).

[61] M. Imada, A. Fujimori, and Y. Tokura, Metal-insulator transitions, Rev. Mod. Phys. **70**, 1039 (1998).

[62] J. Zaanen, G. A. Sawatzky, and J. W. Allen, Band gaps and electronic structure of transition-metal compounds, Phys. Rev. Lett. **55**, 418 (1985).